Chinese Chemical Letters 33 (2022) 762–766

Contents lists available at ScienceDirect

Chinese Chemical Letters

journal homepage: www.elsevier.com/locate/cclet

# Rational design of shortwave infrared (SWIR) fluorescence probe: Cooperation of ICT and ESIPT processes for sensing endogenous cysteine

Maoju Chang, Chenxu Yan*, Lei Shi, Dan Li, Wei Fu, Zhiqian Guo*

*Shanghai Key Laboratory of Functional Materials Chemistry, Key Laboratory for Advanced Materials and Institute of Fine Chemicals, Joint International Research Laboratory of Precision Chemistry and Molecular Engineering, Feringa Nobel Prize Scientist Joint Research Center, Frontiers Science Center for Materiobiology and Dynamic Chemistry, School of Chemistry and Molecular Engineering, East China University of Science and Technology, Shanghai 200237, China*

ARTICLE INFO

*Article history:*
Received 13 May 2021
Revised 24 July 2021
Accepted 5 August 2021
Available online 11 August 2021

*Keywords:*
Fluorescence probe
Shortwave infrared
Intramolecular charge transfer
Excited-state intermolecular proton transfer
Near-infrared

ABSTRACT

Cysteine is well-known to be an important biothiol and related to many diseases. However, the *in vivo* detection of endogenous cysteine still suffers from lacking small-molecule fluorophores with both excitation and emission in the near-infrared (650-900 nm)/shortwave-infrared region. Herein, we report a molecular engineering strategy for shortwave infrared (SWIR, 900-1700 nm) sensing of cysteine, which integrated an excited-state intermolecular proton transfer (ESIPT) building block into the intramolecular charge transfer (ICT) scaffold. The obtained novel fluorophore SH-OH displays a maximum absorption at the NIR region, and emission at the SWIR region. We introduce the cysteine-recognition moiety to SH-OH structure, and demonstrate sensing of endogenous cysteine in living animals, using the SWIR emission as a reliable off-on fluorescence signal. This fluorophore design strategy of cooperation of ICT and ESIPT processes expands the *in vivo* sensing toolbox for accurate analysis in clinical applications.



Biothiols, including glutathione (GSH) [1-3], cysteine (Cys) [4-6], and homocysteine (Hcy) [4], play essential and pervasive roles in physiology, nutrition, and metabolism system [7-10]. Especially, Cys is known to be related to many diseases, including neurotoxicity [11-13], decreased hematopoiesis [14-16], psoriasis, edema, liver damage [17,18], and so on [16-20]. Therefore, *in vivo* sensing of Cys at high spatiotemporal resolution holds the key to the fundamental understanding of its physiological function. Compared to visible (400-600 nm) and near-infrared (NIR, 650-900 nm) light [21-25], shortwave infrared (SWIR, 900-1700 nm) imaging [26-28] allows non-invasive, real-time analysis of biological processes due to low photon scattering, autofluorescence, deeper tissue penetration, and improved signal-background ratio. Thus, there is a desperate need to develop SWIR fluorescence probes that enable high-fidelity *in vivo* sensing of Cys.

Over the last two decades, intramolecular charge transfer (ICT) molecules have been receiving widespread attention for developing activatable fluorophores [29-33]. The ICT reaction can often generate large Stokes shift [34-36] in aromatic dyes possessing strong electron-donor and electron-acceptor substituents, contributing to achieve long-wavelength emission [37,38]. However, the excitations of these ICT fluorophores are still restricted to the visible region. To the best of our knowledge, few studies have been exploited in the small-molecule ICT fluorophores with both excitation and emission in the NIR/SWIR region for *in vivo* imaging. We envision that fluorescence probes uniting ICT and excited-state intermolecular proton transfer (ESIPT) processes [39-42] can realize real-time tracking Cys in the SWIR region.

Herein, we describe a molecular rational design strategy to create activatable off-on SWIR probes for Cys, relying on the cooperation of ICT and ESIPT processes. We employed the "step-by-step" strategy for extending both excitation and emission wavelength: (i) heteroatom substitution (from DCM to SCM building block) for narrowing the energy bandgap in ICT fluorophore scaffold; (ii) employing HBT as an additional ESIPT group [43] for further extending emission wavelength to SWIR region (Fig. 1A). By virtue of harnessing this strategy, a novel small-molecule fluorophore SH-OH was developed with maximum absorption at the NIR region, and emission at the SWIR region. Using the designed probe SHC, we

* Corresponding authors.
*E-mail addresses:* chenxuyan@ecust.edu.cn (C. Yan), guozq@ecust.edu.cn (Z. Guo).

https://doi.org/10.1016/j.cclet.2021.08.015
1001-8417/

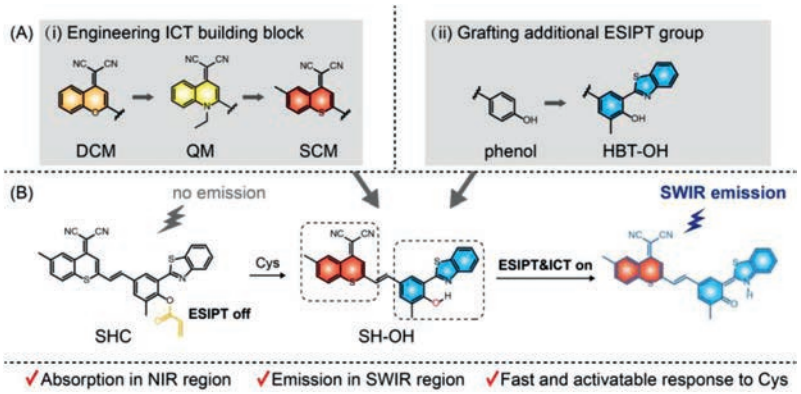


**Fig. 1.** Rational design of shortwave infrared (SWIR) fluorophores for Cys detection. (A) The "step-by-step" strategy to unit ICT and ESIPT processes achieves emission wavelength extension from visible to SWIR region. (i) Engineering ICT building block by heteroatom substitution for narrowing the energy bandgap ($\Delta E_{S1\text{-}S0}$) in ICT fluorophores. (ii) Grafting HBT as additional ESIPT group for further extending emission wavelength to SWIR region. (B) Proposed sensing mechanism of the probe for Cys.

were able to conduct *in vivo* sensing of endogenous Cys *via* the off-on SWIR fluorescence signal (Fig. 1B). This *de novo* strategy for activatable SWIR fluorophores would greatly facilitate the advancement of *in vivo* fluorescence imaging.

We take full advantage of the "step-by-step" strategy to achieve both excitation and emission in the NIR/SWIR region. Above all, we estimated the structure-function relationship between electron-withdrawing building block and emission wavelength. As well known, the DCM group [44-46] has been widely used to construct ICT fluorophores with multiple photophysical advantages, such as adjustable and NIR emission, large Stokes shift, and good photostability [47-49]. In order to further extend the emission wavelength, we replaced the electron-withdrawing building block from QM and DCM to benzothiopyran-malononitrile (SCM) (*i.e.*, replacing the oxygen atom in DCM with sulfur atom). To our delight, the heteroatom substitution led to a significant red-shift in fluorescence spectra. Specifically, QM-OH, DCM-OH, and SCM-OH displayed emission maximums at 560, 685, and 750 nm, respectively (Figs. 2A-C). These results clearly indicated that engineering the SCM as the electron-withdrawing building block could effectively extend the emission wavelength in ICT fluorophores.

To clarify the relationship between the electron-withdrawing building block and fluorescence properties of DCM-OH and SCM-OH, we further carried out density functional theory (DFT) calculation. As determined in Fig. S3 (Supporting information), the energy bandgap ($\Delta E_{S1\text{-}S0}$) of SCM-OH (2.95 eV) is much narrower than that of DCM-OH (3.07 eV), resulting in lower energy for electronic transition and red-shift emission [50]. Simultaneously, the energy of the highest occupied molecular orbital (HOMO) of SCM-OH (–6.070 eV) is higher than that of DCM-OH (–6.108 eV), which means the excited electrons would return to a higher energy state accordingly with a larger Stokes shift [51]. As a consequence, SCM-OH displayed much longer emission and larger Stokes shift than that of DCM-OH (Figs. 2A-C, Fig S1 in Supporting information). Although SCM-OH showed extended emission wavelength in the NIR region, SCM-OH still suffered from the short excitation wavelength ($\lambda_{ex} < 600$ nm, Fig. 2B). In order to develop small-molecule fluorophores with both excitation and emission in the NIR/SWIR region, we then envisioned that fluorescence probes uniting ICT and ESIPT processes could make a breakthrough to further extend the excitation/emission wavelength (Fig. 1B).

To validate the feasibility of this method, we designed and synthesized a novel fluorophore SH-OH by grafting HBT (a typical ESIPT building block) in the SCM-OH scaffold to extend the total $\pi$-conjugation system. Notably, SH-OH showed an obvious absorption peak in the NIR region at 700 nm (Fig. 2B, Fig. S2 in Supporting information). More importantly, SH-OH could emit light in a broad range of 700-1000 nm with a high quantum yield of 2.3 times higher than that of DCM-OH [52] (a NIR fluorophore with high quantum yield, Table S1 in Supporting information), and also exhibited bright emission in the SWIR region (> 900 nm). Taken together, our strategy of uniting ICT and ESIPT mechanism could successfully exploit fluorophores with both excitation and emission wavelength in the NIR/SWIR region.

To further investigate the bio-applicability of SH-OH, we subsequently examined the photostability under physiological conditions, and the results were compared with the commercially available ICG (FDA-proved NIR fluorophore). As depicted in Fig. 2D, the fluorescence intensity of commercial dye ICG dropped rapidly to 1% after irradiation for 10 min under stable light irradiation, indicating that ICG was photobleached. Meanwhile, the fluorescence intensity of SH-OH, SCM-OH, and DCM-OH decreased to 47%, 48%, and 42%, respectively. Clearly, SH-OH exhibited higher photostability than ICG, enabling its much longer time-lapse imaging [53]. All these data demonstrated that SH-OH could be utilized as an excellent SWIR fluorophore for *in vivo* bioimaging applications.

As well known, the fluorescence intensities of ICT chromophores are extremely sensitive to electronic disturbance [29,30]. For an example of SCM-OH, after masking the hydroxyl group with electron-withdrawing acryloyl group, the NIR fluorescence intensity of SCM-OH was effectively quenched (Figs. 3A and B). In the presence of Cys, the acryloyl group of SOC was cleavaged, and the released SCM-$O^-$ could lead to a significant fluorescence enhancement (Figs. 3A-E, Figs. S5 and S6 in Supporting information). Encouraged by this fluorescence response, we further explored the feasibility to employ SH-OH (fluorophore uniting ICT and ESIPT) as an activatable SWIR fluorophore.

We subsequently evaluated the pH dependence of the emission profiles of SH-OH and acryloyl group masked SHC. As shown in Fig. S4 (Supporting information), the SWIR fluorescence of SHC remained silent over the physiological pH range. Importantly, the p$K_a$ of SH-OH was measured to be *ca.* 7.8 (Fig. S4), which allowed SHC to favorably exploit the physiological conditions of living systems.

The pH-insensitivity of SHC and pH-sensitivity of SH-OH inspired us to further test the validity of this probe *in vitro* and *in vivo*. As demonstrated in Figs. 3F and G. The probe SHC performed an obvious fluorescence signal in the SWIR region in the presence of Cys as the acryloyl group of SHC was cleavage and SH-$O^-$ was released (Fig. S7 in Supporting information). This Cys-triggered reaction reached equilibrium in only 5 min (Fig. 3G), indicating a very fast response toward Cys. Notably, the plots of the $I_{950\ nm}$ against the concentrations of Cys ranging from 0 to 100 μm displayed a good linear relationship (Figs. 3I and J). Hence, the linear curve of the $I_{950\ nm}$ allowed for the convenient quantitative

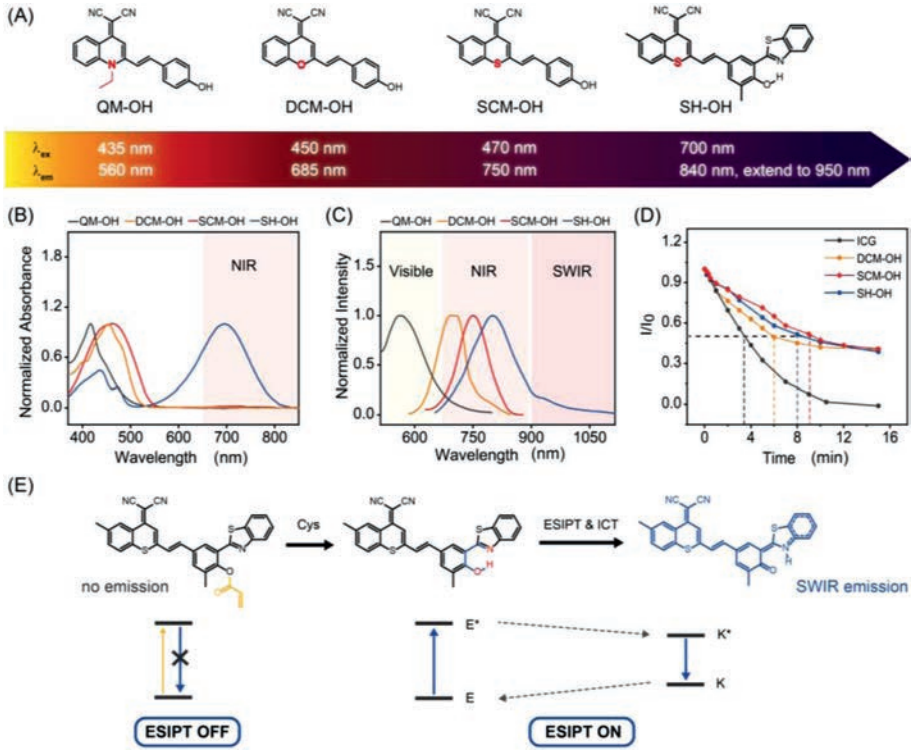


**Fig. 2.** Engineering SCM fluorophores with absorption in NIR region and emission in SWIR region. (A) Chemical structures, excitation peaks and emission peaks of QM-OH, DCM-OH, SCM-OH, and SH-OH. (B) Normalized absorption spectra in DMSO and (C) normalized fluorescence spectra of QM-OH, DCM-OH, SCM-OH, and SH-OH. (D) Time-dependent normalized fluorescence intensity of SH-OH (monitored at 840 nm, $\lambda_{ex}$ = 600 nm), SCM-OH (monitored at 750 nm, $\lambda_{ex}$ = 595 nm), DCM-OH (monitored at 685 nm, $\lambda_{ex}$ = 560 nm), and ICG (monitored at 812 nm, $\lambda_{ex}$ = 780 nm) under sustained illumination. (E) Design of SWIR activatable probe SHC for detection of Cys.

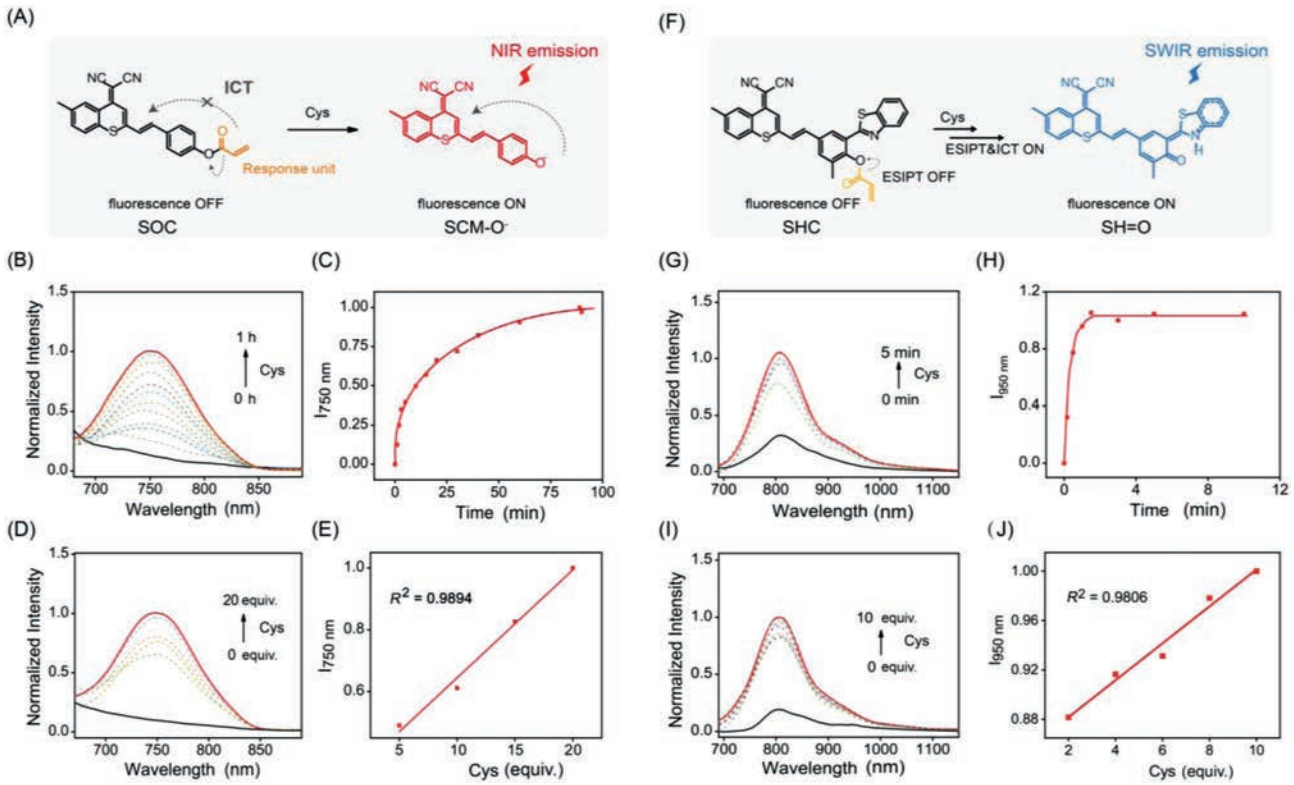


**Fig. 3.** Cys-triggered fluorescence response in SWIR region. (A) Proposed mechanism of SOC incubated with Cys. (B) Time-dependent normalized fluorescence spectra of SOC (100 μmol/L) incubation with Cys (20 equiv.). (C) Time-dependent normalized $I_{750\ nm}$ of SOC with Cys (20 equiv.). (D) Normalized fluorescence spectra of SOC upon treatment with consequent concentration Cys after reacting 1 h at 37 °C. (E) The relationship between normalized $I_{750\ nm}$ of SOC and Cys concentration after incubation with 1 h. (F) Proposed mechanism of SHC incubated with Cys. (G) Time-dependent normalized fluorescence spectra of SHC (10 μmol/L) incubation with Cys (10 equiv.). (H) Time-dependent normalized $I_{950\ nm}$ of SHC with Cys (10 equiv.). (I) Normalized fluorescence spectra of SHC upon treatment with consequent concentration Cys after reacting 5 min at 37 °C. (J) The relationship of normalized $I_{950\ nm}$ of SHC and Cys concentration after incubation with 5 min.

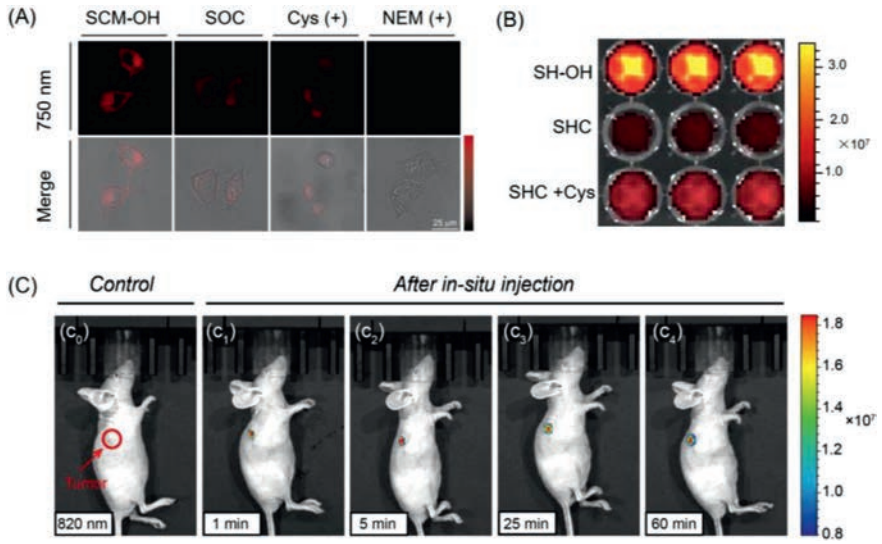


**Fig. 4.** *In vitro* and *in vivo* bioimaging. (A) Confocal laser scanning microscope (CLSM) images of HeLa cells incubated with different compounds (100 μmol/L) for 1 h such as SCM-OH, probe SOC, exogenous Cys and SOC, NEM and SOC. Note: the NIR fluorescence intensity monitored channel obtained from 740 nm to 760 nm, $\lambda_{ex}$ = 605 nm. (B) Plate fluorescence imaging of SH-OH (10 μmol/L), probe SHC (10 μmol/L) and SHC (10 μmol/L) incubating with Cys (100 μmol/L), yellow-red scale. (C) *In vivo* SWIR fluorescence imaging of HeLa xenograft mice after *in situ* injection of SHC probe at various time (1 min, $c_1$; 5 min, $c_2$; 25 min, $c_3$; 60 min, $c_4$), rainbow scale. Note: $\lambda_{ex}$ = 600 nm, SWIR fluorescence signal monitored at 950 nm.

detection of Cys over this concentration range. Besides, the detection limit of the probe SHC was 4 μmol/L, indicating excellent sensitivity of SHC toward Cys (Table S2 in Supporting information). Consequently, SHC enabled the fast and quantitative SWIR fluorescence detection of Cys.

The complex microenvironment *in vivo* could affect the recognition and efficiency of fluorescence probes on the target analyte. Hence, the selectivity of the probe is one of the key indicators to evaluate the application in biological samples. To our satisfaction, both SOC and SHC exhibited a significantly higher selectivity toward Cys than any other biothiols such as glutathione (Figs. S8 and S9 in Supporting information). When glutamic or other amino acids were added to the solution, the fluorescence intensity of SHC showed little change. In contrast, the signal at 950 nm apparently increased after incubating with Cys for 5 min, thereby verifying that probe SHC exerted outstanding selectivity to Cys. Overall, we have successfully developed and demonstrated a viable strategy for the SWIR fluorescence analysis of Cys.

As demonstrated, SHC exhibited activatable SWIR fluorescence toward Cys, while SOC displayed an activatable NIR fluorescence. This SWIR imaging has advantages over NIR imaging *in vivo* due to deeper tissue penetration. Therefore, SOC/SHC has great potential for *in vitro* and *in vivo* bioimaging, respectively. Subsequently, HeLa cells were selected to evaluate the response of the probe SOC to exogenous and endogenous Cys *in vitro*. Compared to the HeLa cells incubated with SCM-OH for 1 h at 37 °C, the NIR signal in the 740-760 nm fluorescence channel exhibited observable signal when treated with SOC (Fig. 4A). It suggested that SOC could sense endogenous Cys in cells. Besides, when pretreated with exogenous Cys for promotion intracellular Cys concentration, the signal was observed obviously. On the other hand, in order to verify the specific recognition of Cys by SOC, we pretreated HeLa cells with NEM, the Cys inhibitor, to inhibit the expression of Cys in cells [54]. As expected, the confocal laser scanning microscope (CLSM) image revealed a negligible detection signal in cells. The above results demonstrated effective fluorescence "turn-on" detection of probe SOC in the presence of either exogenous or endogenous Cys *in vitro*. Therefore, we have successfully achieved a light-up NIR probe SOC for the detection and imaging of Cys in living cells.

Considered that the SWIR signal possesses deeper tissue penetration, and improved signal-background ratio than that of the NIR signal, the PerkinElmer IVIS spectrum was executed to assess the *in vivo* performance of SHC as a Cys-triggered SWIR probe. As shown in Fig. 4B, the fluorescence signal at the SWIR region of the plate with SHC could be negligible in PBS/DMSO mixture solution. In contrast, when treated with Cys for 5 min, the signal emerged and could clearly be observed. Afterward, we investigated the capability of SHC for real-time *in vivo* visualization of Cys activity in tumors (Fig. 4C). When the nude mice were intratumor injected with probe SHC, SHC displayed a remarkable fluorescence signal at SWIR region immediately, indicated that SHC was activated rapidly by endogenous Cys. Furthermore, the SWIR fluorescence signal could still be observed after injecting 1 h (Fig. S10 in Supporting information), which demonstrated SHC could achieve long-term tracking of endogenous Cys activity *in vivo*. These imaging results further highlight the potential of SHC for *in vivo* sensing of Cys in the SWIR region.

In summary, we focused on engineering long-wavelength fluorophores for reliable SWIR imaging of Cys *in vivo*. We have successfully developed a molecular engineering strategy with the cooperation of ICT and ESIPT processes that enabled to construct chromophores with both excitation and emission in the NIR/SWIR region. By employing the "step-by-step" strategy, we rationally engineered the electron-withdrawing building block from DCM to SCM, and grafted HBT in the SCM-based ICT scaffold. The obtained SH-OH displayed a maximum absorption at the NIR region, emission at the SWIR region, large Stokes shift, and excellent photostability. The combination of the SWIR emission and activatable response allows construction of fluorescence probe SHC that can be applied for reliable sensing of Cys both *in vitro* and *in vivo*. We anticipate that our strategy of uniting ICT and ESIPT processes would inspire the creation of a generation of quantitative SWIR fluorescence assays for clinical applications.

## Declaration of competing interest

The authors declare that they have no known competing financial interests or personal relationships that could have appeared to influence the work reported in this paper.

## Acknowledgments

This work was supported by the National Natural Science Foundation of China (Nos. 21878087, 21908060), the Innovation Program of Shanghai Municipal Education Commission, Shuguang Program (No. 18SG27). This study was performed in strict accordance with the NIH guidelines for the care and use of laboratory animals (NIH Publication No. 85-23, Rev. 1985) and was approved by the Institutional Animal Care and Use Committee of National Tissue Engineering Center (Shanghai, China).

## Supplementary materials

Supplementary material associated with this article can be found, in the online version, at doi:10.1016/j.cclet.2021.08.015.

## References

[1] H. Zong, J. Peng, T.D. James, et al., Chem. Commun. 56 (2020) 515–518.
[2] L. Wu, J. Yoon, J.L. Sessler, T.D. James, et al., Chem. Soc. Rev. 49 (2020) 5110–5139.
[3] D. Li, W. Chen, J. Yin, et al., Chin. Chem. Lett. 31 (2020) 2891–2896.
[4] H. Xu, W. Wang, K. Lou, et al., Anal. Chem. 92 (2020) 13829–13838.
[5] L. Wu, J. Liu, P. Li, B. Tang, T.D. James, Chem. Soc. Rev. 50 (2021) 702–734.
[6] Z. Liu, X. Wu, J. Yoon, et al., Angew. Chem. Int. Ed. 56 (2017) 5812–5816.
[7] X.L. Hu, A.C. Sedgwick, J. Yoon, et al., Adv. Funct. Mater. 30 (2020) 1907906.
[8] Z. Xu, Y. Tan, J. Yin, et al., Anal. Chem. 91 (2019) 11343–11348.
[9] L. Li, H. Chen, J. Yin, et al., Chin. Chem. Lett. 30 (2019) 1689–1703.
[10] H. Li, J. Wang, J. Yoon, et al., Angew. Chem. Int. Ed. 59 (2020) 10186–10195.
[11] Q.Y. Cao, J.S. Kim, et al., Chem. Commun. 56 (2020) 10317–10320.
[12] X. Xu, X. Zhou, J. Tang, et al., Nano Lett. 21 (2021) 2199–2206.
[13] M. Won, A. Sharma, J.S. Kim, et al., Angew. Chem. Int. Ed. 60 (2021) 3196–3204.
[14] J. Wang, S. Hu, Y. Shen, et al., Adv. Funct. Mater. 29 (2019) 1807446.
[15] J. Li, Y. Fang, D. Ding, et al., Adv. Mater. 33 (2021) 2008518.
[16] X. Yi, F. Xia, B.Z. Tang, et al., ACS Nano 15 (2021) 3026–3037.
[17] D. Yan, Q. Wu, D. Wang, B.Z. Tang, Angew. Chem. Int. Ed. 60 (2021) 15724–15742.
[18] Y. Ning, J.L. Sessler, J.L. Zhang, et al., J. Am. Chem. Soc. 142 (2020) 6761–6768.
[19] X.Q. Yu, C. Sun, G.C. Guo, et al., Nat. Commun. 11 (2020) 1179.
[20] S. Banerji, M. Meem, R. Menon, et al., OSA Continuum 2 (2019) 1199–1206.
[21] N. Li, Z. Lan, F. Zhu, et al., Adv. Sci. 7 (2020) 2000444.
[22] O. Juan, L. Sun, S.Z. Wu, Angew. Chem. Int. Ed. 59 (2020) 10111–10121.
[23] J. Chem, F. Zeng, S.Z. Wu, et al., Chem. Commun. 56 (2020) 11102–11105.
[24] C. Chen, X. Ni, D. Ding, et al., Adv. Mater. 31 (2019) 1904914.
[25] X. Ni, X. Zhang, D. Ding, et al., Nano. Lett. 19 (2019) 318–330.
[26] S. Lu, X. Lei, X. Chen, et al., ACS Appl. Bio Mater. 3 (2020) 3835–3845.
[27] L. Wu, B. Tang, T.D. James, et al., Chem. Sci. 12 (2021) 3921–3928.
[28] X. Tian, S.E. Lewis, T.D. James, et al., Chem Sci 12 (2021) 3406–3426.
[29] J. Ning, X. Ma, T.D. James, et al., Angew. Chem. Int. Ed. 58 (2019) 9959–9963.
[30] L.C. Murfin, T.D. James, S.E. Lewis, et al., J. Am. Chem. Soc. 141 (2019) 19389–19396.
[31] Y. Gao, Y. Hu, T.D. James, Y. Guo, et al., Angew. Chem. Int. Ed. 60 (2021) 10756–10765.
[32] S. Shanmugaraju, G.W. Watson, T. Gunnlaugsson, et al., Chem. Commun. 55 (2019) 12140–12143.
[33] C. Chen, X. Ni, D. Ding, et al., Angew. Chem. Int. Ed. 59 (2020) 10008–10012.
[34] R.M. Duke, E.B. Veale, T. Gunnlaugsson, et al., Chem. Soc. Rev. 39 (2010) 3936–3953.
[35] V.N. Nguyen, S. Park, J. Yoon, et al., Angew. Chem. Int. Ed. 59 (2020) 8957–8962.
[36] C. Yan, Y. Zhang, Z. Guo, Chin. Chem. Lett. 30 (2019) 839–846.
[37] J. Wu, L. Jiang, J.S. Kim, et al., Chem. Commun. 55 (2019) 9947–9950.
[38] S.Y. Park, M. Won, J.S. Kim, et al., Sens. Actuators B: Chem. 319 (2020) 128306.
[39] W. Zhou, X. Fang, Z. Xu, et al., Chin. Chem. Lett. 32 (2021) 943–946.
[40] D. Wu, L. Chen, Q. Xu, J. Yoon, et al., Acc. Chem. Res. 52 (2019) 2158–2168.
[41] H. Feng, D. Ding, B.Z. Zhong, et al., J. Am. Chem. Soc. 37 (2020) 15966–15974.
[42] Y. Chen, Y. Fang, X. Chen, et al., ACS Appl. Mater. Interfaces 12 (2020) 55094–55106.
[43] C. Yan, Y. Zhang, Z. Guo, Coord. Chem. Rev. 427 (2021) 213556.
[44] K.C. Yan, A.C. Sedgwick, T.D. James, et al., Small Methods 3 (2019) 1900013.
[45] M.L. Odyniec, S.J. Park, T.D. James, et al., Chem. Sci. 11 (2020) 7329–7334.
[46] J.H. Joo, J.S. Kim, M.H. Lee, et al., Sens. Actuators B: Chem. 320 (2020) 128360.
[47] C. Yan, J. Tang, Z. Guo, et al., Sci. China Chem. 64 (2021) 2045–2052.
[48] H. Ren, F. Huo, C. Yin, et al., Chem. Commun. 57 (2021) 655–658.
[49] W. Chen, C. Zhang, J. Yin, et al., Anal. Chem. 93 (2021) 3378–3385.
[50] G. Feng, G. Zhang, D. Ding, Chem. Soc. Rev. 49 (2020) 8179–8234.
[51] T.B. Ren, L. Yuan, X.B. Zhang, et al., J. Am. Chem. Soc. 140 (2018) 7716–7722.
[52] K. Gu, Z. Guo, W.H. Zhu, et al., J. Am. Chem. Soc. 138 (2016) 5334–5340.
[53] C. Tang, S. Vanslyke, C. Chen, et al., J. Appl. Phys. 85 (1989) 3610.
[54] X. Xie, C. Yin, F. Huo, et al., Sens. Actuators B: Chem. 267 (2018) 76–82.